American Mineralogist, Volume 62, pages 921–931, 1977

A high-temperature study of the thermal expansion and the anisotropy of the sodium atom in low albite

JOHN K. WINTER, SUBRATA GHOSE AND FUJIO P. OKAMURA[1]

Department of Geological Sciences
University of Washington, Seattle, Washington 98195

Abstract

The crystal structure of albite from Tiburon, Marin County, California, has been refined from three-dimensional X-ray intensity data collected on an automatic single-crystal diffractometer at 500, 750, and 970°C (all ±10°C) to *R* factors of 0.032, 0.035, and 0.039 for 1980, 1990, and 2002 reflections respectively. The vibrational amplitude of the sodium atom exhibits a linear dependence on temperature and extrapolates to zero at 0 K within error limits, implying that the high anisotropy of the electron-density distribution about the Na position is strictly a result of anisotropic thermal motion. Structural adjustments to thermally induced stresses are principally associated with *T*–O–*T* angles as opposed to distortion within the aluminosilicate tetrahedra. Whereas Na–O bond lengths increase substantially with increasing temperature, the *T*–O bond lengths show little change. The apparent slight shortening of the *T*–O bonds is attributed to errors in bond-length calculation caused by thermal motion.

Introduction

The electron density at the sodium atom position in both high and low albite is markedly anisotropic, the effect being much larger in high albite. The anisotropy of the sodium atom has been discussed by Ferguson *et al.* (1958), Williams and Megaw (1964), and Smith (1974). Two possible explanations for this phenomenon are: (1) a time average of highly anistropic thermal vibration of sodium within the aluminosilicate cage; or (2) a space average of multiple positions occupied by the sodium atom. Multiple positions may occur in either of two ways. There may be two or more positions of low potential energy with sodium atoms occupying different ones or oscillating between them. Another possibility is the existence of a multipartite structure of fault-bounded domains.

Distinguishing between a time average and a space average using electron-density maps can be quite difficult, since the separation of the two positions must be large enough to show up as two distinct peaks. If the separation is smaller than some critical distance, the overlap will appear as a single elongated peak. This problem has been discussed in some detail by Megaw in an appendix to Ribbe *et al.* (1969). A superior approach is to observe the behavior of the Na atom at a variety of temperatures. Whereas a space average would show little variation with temperature, thermal vibrations should decrease with decreasing temperature and eventually reduce to zero at 0 K. Initial work along these lines was conducted by Williams and Megaw (1964) at −180°C and by Quareni and Taylor (1971) at 300 and 600°C, who used two-dimensional Weissenberg data with intensities measured by multiple film techniques. The results of refinement based on more complete and accurate three-dimensional intensity data are needed to confirm these initial results. Some high-temperature data have been collected by Prewitt *et al.* (1974), but no structural details on low albite are available.

Experimental

In order to collect intensity data at high temperatures, a Pt-resistance microfurnace was constructed to fit the 9-inch diameter χ circle of a Syntex $P\bar{1}$ 4-circle diffractometer. Calibration against the thermal expansion of quartz and the melting points of $Ba(NO_3)_2$, NaCl, and Au was reproducible to within 10°C. However, the temperature at $\chi = 0$ was 14°C higher than at $\chi = 90$ and 180 degrees. In this position the furnace is inverted and convection is im-

[1] Present address: National Institute for Researches in Inorganic Materials, Kurakake, Sakura-mura, Niihari-gun, Ibaraki 300-31, Japan.

Table 1. Tiburon low albite: cell dimensions as a function of temperature

	25°C	250°C	500°C		750°C		970°C	
		Incr. T	Incr. T	Decr. T	Incr. T	Decr. T	Incr. T	Decr. T
a (Å)	8.152(1)	8.175(1)	8.206(1)	8.205(1)	8.242(1)	8.244(1)	8.277(1)	8.281(1)
b (Å)	12.784(3)	12.798(3)	12.817(3)	12.817(3)	12.841(2)	12.841(3)	12.860(2)	12.862(2)
c (Å)	7.165(1)	7.166(1)	7.169(1)	7.169(1)	7.176(1)	7.175(1)	7.181(1)	7.182(1)
α (°)	94.28(2)	94.18(2)	93.99(2)	93.97(2)	93.69(1)	93.65(2)	93.33(1)	93.29(1)
β (°)	116.67(1)	116.54(1)	116.39(1)	116.39(1)	116.27(1)	116.25(1)	116.15(1)	116.14(1)
γ (°)	87.74(2)	87.72(2)	87.68(2)	87.69(2)	87.62(1)	87.62(1)	87.56(1)	87.56(1)
V (Å^3)	665.4(2)	669.0(2)	673.8(2)	673.7(2)	679.6(2)	679.8(2)	684.9(2)	685.4(2)

paired. Lacking the equipment to compensate for temperature variations as a function of the χ angle, this inaccuracy had to be tolerated.

Tiburon albite ($Ab_{99.75}$ $Or_{0.25}$) was chosen for these experiments for its purity. A sample of suitable crystallinity, checked by transmission Laue photographs, was ground to a nearly spherical shape of 0.25 mm diameter using a sphere grinder (Bond, 1951). The crystal sphere was mounted in a silica-glass capillary using a cement of ground mullite and a binder ("Zircoabond 6" by Zircoa Corp.). The capillary was then evacuated and sealed. Intensities of 1980, 1990, and 2002 reflections were measured at 500, 750, and 970°C respectively, using the ω-2θ method on the diffractometer, with Mo$K\alpha$ radiation monochromatized by reflection from a graphite "single" crystal, and a scintillation counter. A variable scan rate was used, the minimum being 2°/min. Unfortunately, while cooling from 250°C to room temperature, the capillary fractured as a result of thermal stresses. The crystal was lost; thus, post-analysis compositional data and room-temperarature refinement are lacking. For the present, Wainwright's room temperature data on Tiburon albite [in Smith (1974)] are being used.

The intensity data were corrected for Lorentz, polarization, and absorption effects. The glass of the capillary and the furnace were of nearly constant thickness (0.02–0.03 mm). Several widely spaced diopside reflections were collected with and without the furnace enclosure. Absorption effects were constant within counting error. Hence the absorption effects due to the glass of the capillary and the furnace enclosure were neglected. Least-squares refinement of the structure was intiated using the RFINE program (Finger, 1969). The atomic scattering factors of Na, Al, Si, and O were taken from Cromer and Mann (1968). Anomalous dispersion corrections were made according to Cromer and Liberman (1970). The observed structure factors (F_o's) were weighted by $1/\sigma^2(F_o)$, where $\sigma(F_o)$ is the standard deviation of F_o, as measured by the counting statistics. Four cycles of refinement using isotropic temperature factors resulted in R factors of 0.090, 0.087, and 0.104 for 500, 750, and 970°C respectively. A further five refinement cycles using anisotropic temperature factors were required to achieve convergence. The final R factors are 0.032, 0.035, and 0.039 for the same respective temperatures. Cell dimensions, atomic coordinates, and thermal ellipsoid parameters are listed in Tables 1, 2, and 3 respectively. Table 4[2] lists the observed and calculated structure factors. Polynomial regression equations to the first and second order have been fitted to all temperature-dependent data, and the coefficients are listed in the appendix. Bond distances and angles are listed in Tables 5 and 6.

Results and discussion

Cell dimensions, strain ellipsoids and atomic parameters as a function of temperature

The cell dimensions were measured at room temperature and 250°C as well as at 500, 750, and 970°C prior to data collection and remeasured upon cooling. No hysteresis effects were observed. The axial dimensions and cell volume all increase with increasing temperature (Fig. 1). However, for monoclinic and triclinic crystals, the cell expansion in terms of the axial dimensions can be misleading, as the princi-

[2] To obtain a copy of this table, order document AM-77-053 from the Business Office, 1909 K Street, N.W., Washington, D. C. 20006. Please remit $1.00 in advance for the microfiche.

Table 2. Tiburon low albite: atomic coordinates and anisotropic temperature factors as a function of temperature

		25°C*	500°C	750°C	970°C
Na	x	.2683	.2735(2)	.2759(2)	.2782(3)
	y	.9890	.9881(2)	.9882(2)	.9883(2)
	z	.1463	.1470(3)	.1466(3)	.1468(4)
	β_{11}		.0136(3)	.0184(3)	.0236(5)
	β_{22}		.0135(2)	.0174(2)	.0203(3)
	β_{33}		.0379(6)	.0487(7)	.0612(9)
	β_{12}		-.0019(2)	-.0024(2)	-.0020(3)
	β_{13}		.0082(3)	.0105(4)	.0137(5)
	β_{23}		-.0112(3)	-.0131(3)	-.0124(4)
$T_1(o)$	x	.0089	.0091(1)	.0094(1)	.0098(1)
	y	.1682	.1710(1)	.1727(1)	.1747(1)
	z	.2080	.2092(1)	.2102(1)	.2113(1)
	β_{11}		.0069(1)	.0089(1)	.0111(1)
	β_{22}		.0020(0)	.0026(1)	.0032(1)
	β_{33}		.0071(1)	.0092(1)	.0113(2)
	β_{12}		-.0006(0)	-.0008(1)	-.0010(1)
	β_{13}		.0031(1)	.0040(1)	.0050(1)
	β_{23}		.0001(1)	.0002(1)	.0002(1)
$T_1(m)$	x	.0037	.0046(1)	.0051(1)	.0058(1)
	y	.8205	.8198(1)	.8198(1)	.8200(1)
	z	.2374	.2375(1)	.2372(1)	.2370(1)
	β_{11}		.0063(1)	.0082(1)	.0101(1)
	β_{22}		.0018(0)	.0024(1)	.0030(1)
	β_{33}		.0065(1)	.0084(1)	.0102(1)
	β_{12}		.0005(0)	.0007(1)	.0008(1)
	β_{13}		.0030(1)	.0039(1)	.0047(1)
	β_{23}		.0005(0)	.0005(1)	.0005(1)
$T_2(o)$	x	.6917	.6952(1)	.6974(1)	.6997(1)
	y	.1102	.1114(1)	.1124(1)	.1135(1)
	z	.3147	.3192(1)	.3221(1)	.3252(1)
	β_{11}		.0057(1)	.0075(1)	.0092(1)
	β_{22}		.0015(0)	.0020(1)	.0025(1)
	β_{33}		.0083(1)	.0109(1)	.0136(1)
	β_{12}		-.0003(1)	-.0004(1)	-.0005(1)
	β_{13}		.0024(1)	.0032(1)	.0040(1)
	β_{23}		.0002(0)	.0002(1)	.0002(1)
$T_2(m)$	x	.6815	.6860(1)	.6886(1)	.6911(1)
	y	.8818	.8822(1)	.8826(1)	.8830(1)
	z	.3607	.3610(1)	.3605(1)	.3596(1)
	β_{11}		.0057(1)	.0074(1)	.0091(1)
	β_{22}		.0015(1)	.0020(1)	.0025(1)
	β_{33}		.0086(1)	.0113(1)	.0139(1)
	β_{12}		.0002(1)	.0002(1)	.0002(1)
	β_{13}		.0027(1)	.0036(1)	.0044(1)
	β_{23}		.0005(1)	.0006(1)	.0006(1)
O_{A1}	x	.0048	.0051(3)	.0049(3)	.0045(3)
	y	.1312	.1345(1)	.1359(1)	.1371(2)
	z	.9662	.9686(3)	.9703(3)	.9717(3)
	β_{11}		.0152(4)	.0198(4)	.0242(1)
	β_{22}		.0036(1)	.0048(1)	.0061(1)
	β_{33}		.0087(4)	.0108(4)	.0133(4)
	β_{12}		-.0003(2)	-.0004(2)	-.0002(2)
	β_{13}		.0067(3)	.0086(3)	.0106(4)
	β_{23}		.0007(2)	.0009(2)	.0011(2)
O_{A2}	x	.5922	.5995(2)	.6038(2)	.6078(2)
	y	.9973	.9983(1)	.9993(1)	.0001(3)
	z	.2809	.2830(3)	.2841(3)	.2841(3)
	β_{11}		.0071(3)	.0090(3)	.0117(3)
	β_{22}		.0016(1)	.0021(1)	.0025(1)
	β_{33}		.0140(4)	.0189(4)	.0230(5)
	β_{12}		-.0001(1)	-.0001(1)	-.0002(1)
	β_{13}		.0029(3)	.0034(3)	.0043(3)
	β_{23}		.0009(1)	.0012(1)	.0012(2)
$O_B(o)$	x	.8125	.8132(2)	.8140(3)	.8155(3)
	y	.1099	.1149(1)	.1186(1)	.1223(2)
	z	.1902	.1941(3)	.1967(3)	.2012(4)
	β_{11}		.0105(3)	.0136(4)	.0164(4)
	β_{22}		.0042(1)	.0056(1)	.0073(2)
	β_{33}		.0175(5)	.0226(5)	.0282(6)
	β_{12}		-.0021(2)	-.0027(2)	-.0034(2)
	β_{13}		.0085(3)	.0111(4)	.0137(4)
	β_{23}		-.0008(1)	-.0008(2)	-.0005(3)
$O_B(m)$	x	.8196	.8219(3)	.8233(3)	.8252(3)
	y	.8512	.8512(2)	.8520(2)	.8531(3)
	z	.2583	.2563(3)	.2555(4)	.2549(4)
	β_{11}		.0120(4)	.0154(4)	.0178(5)
	β_{22}		.0049(1)	.0065(2)	.0081(2)
	β_{33}		.0241(6)	.0307(7)	.0359(8)
	β_{12}		.0020(2)	.0029(2)	.0031(2)
	β_{13}		.0122(4)	.0155(5)	.0175(5)
	β_{23}		.0009(2)	.0011(3)	.0009(3)
$O_C(o)$	x	.0128	.0179(2)	.0203(2)	.0225(3)
	y	.3012	.3045(1)	.3062(1)	.3080(1)
	z	.2708	.2705(3)	.2696(3)	.2679(3)
	β_{11}		.0094(3)	.0123(3)	.0151(4)
	β_{22}		.0022(1)	.0028(1)	.0036(1)
	β_{33}		.0175(5)	.0231(5)	.0285(6)
	β_{12}		-.0012(1)	-.0017(1)	-.0019(2)
	β_{13}		.0048(3)	.0062(3)	.0074(4)
	β_{23}		-.0005(2)	-.0009(2)	-.0007(2)
$O_C(m)$	x	.0239	.0257(2)	.0275(2)	.0298(3)
	y	.6939	.6937(1)	.6940(1)	.6947(1)
	z	.2291	.2369(3)	.2413(3)	.2466(3)
	β_{11}		.0092(3)	.0123(3)	.0152(4)
	β_{22}		.0020(1)	.0027(1)	.0033(1)
	β_{33}		.0167(4)	.0220(5)	.0290(6)
	β_{12}		.0011(1)	.0015(1)	.0021(2)
	β_{13}		.0034(3)	.0050(3)	.0074(4)
	β_{23}		.0008(2)	.0010(2)	.0018(2)
$O_D(o)$	x	.2073	.2045(2)	.2029(3)	.2014(3)
	y	.1089	.1106(1)	.1119(1)	.1136(2)
	z	.3891	.3905(3)	.3921(3)	.3934(3)
	β_{11}		.0114(3)	.0147(4)	.0175(4)
	β_{22}		.0037(1)	.0050(1)	.0061(1)
	β_{33}		.0093(4)	.0124(4)	.0152(5)
	β_{12}		.0011(2)	.0013(2)	.0015(2)
	β_{13}		.0013(3)	.0018(3)	.0023(4)
	β_{23}		.0009(2)	.0013(2)	.0016(2)
$O_D(m)$	x	.1840	.1816(3)	.1808(3)	.1795(3)
	y	.8681	.8688(1)	.8694(2)	.8706(2)
	z	.4368	.4330(3)	.4301(3)	.4280(3)
	β_{11}		.0125(3)	.0162(4)	.0190(5)
	β_{22}		.0041(1)	.0053(1)	.0068(2)
	β_{33}		.0096(4)	.0124(4)	.0153(5)
	β_{12}		-.0013(2)	-.0020(2)	-.0023(2)
	β_{13}		.0000(3)	.0004(3)	.0006(4)
	β_{23}		-.0005(2)	-.0008(2)	-.0007(2)

*Data from Wainwright (in Smith, 1974)

pal expansion directions may deviate significantly from the axial directions. Thermal strain ellipsoids of feldspars have been calculated by Ohashi and Finger (1973) and by Willaime *et al.* (1974). Dr. Finger has graciously computed the strain ellipsoids based on our unit-cell data measured at 25, 500, 750, and 970°C using his program STRAIN. The results, shown in Table 7 and Figure 3, agree quite well with previous studies.

Table 3. Tiburon low albite: anisotropic thermal ellipsoid, axial lengths, and isotropic equivalent temperature factors as a function of temperature

		−180°C+	25°C*	500°C	750°C	970°C
Na	R_1		.119(2)	.189	.222	.256
	R_2		.173(2)	.217	.259	.306
	R_3		.248(3)	.399	.446	.472
	B	1.0(3)	2.33	6.37	8.29	10.05
$T_1(o)$	R_1			.119	.136	.151
	R_2			.122	.140	.156
	R_3			.144	.165	.185
	B	0.15(6)	0.54(1)	1.31	1.72	2.14
$T_1(m)$	R_1			.113	.130	.144
	R_2			.117	.134	.149
	R_3			.138	.159	.178
	B		0.55(1)	1.20	1.58	1.97
$T_2(o)$	R_1			.110	.127	.141
	R_2			.124	.143	.160
	R_3			.140	.160	.178
	B		0.51(1)	1.24	1.64	2.03
$T_2(m)$	R_1			.111	.128	.142
	R_2			.126	.145	.161
	R_3			.137	.158	.175
	B	0.18(6) (ave. Si)	0.52(1)	1.23	1.63	2.02
O_{A1}	R_1		.093(4)	.119	.133	.148
	R_2		.111(4)	.172	.200	.226
	R_3		.145(4)	.205	.235	.261
	B		0.99(1)	2.25	2.97	3.72
O_{A2}	R_1		.073(4)	.113	.128	.143
	R_2		.093(2)	.138	.156	.179
	R_3		.128(4)	.184	.216	.240
	B		0.73(1)	1.73	2.30	2.89
$O_B(o)$	R_1		.106(3)	.132	.148	.161
	R_2		.123(2)	.176	.205	.236
	R_3		.136(4)	.212	.241	.268
	B		1.02(1)	2.45	3.22	4.05
$O_B(m)$	R_1		.120(3)	.126	.142	.159
	R_2		.139(3)	.208	.240	.268
	R_3		.153(4)	.230	.263	.284
	B		1.29(1)	2.96	3.88	4.67
$O_C(o)$	R_1		.090(4)	.124	.138	.160
	R_2		.109(1)	.169	.195	.215
	R_3		.144(5)	.198	.229	.255
	B		0.97(1)	2.18	2.88	3.60
$O_C(m)$	R_1		.088(4)	.119	.136	.149
	R_2		.106(3)	.164	.193	.220
	R_3		.146(4)	.204	.231	.257
	B		0.93(1)	2.17	2.86	3.60
$O_D(o)$	R_1		.089(3)	.129	.148	.165
	R_2		.115(4)	.174	.202	.225
	R_3		.137(4)	.210	.238	.260
	B		1.01(1)	2.39	3.14	3.82
$O_D(m)$	R_1		.090(3)	.125	.143	.161
	R_2		.116(4)	.188	.212	.237
	R_3		.150(4)	.225	.255	.279
	B	0.38(6)	1.14(1)	2.67	3.44	4.22

+ Data from Williams and Megaw (1964): re-refined by Quareni and Taylor (1971)
* Data from Wainwright (in Smith, 1974)

Table 5. Tiburon low albite: Na–O and *T*–O bond lengths as a function of temperature

	25°C*	500°C	750°C	970°C
Na–O_{A1}	2.669	2.739(3)	2.765(3)	2.788(3)
–O_{A1}	2.535	2.609(2)	2.649(3)	2.684(3)
–O_{A2}	2.369	2.412(2)	2.439(2)	2.467(3)
–O_B(o)	2.454	2.511(2)	2.556(3)	2.616(3)
–O_C(o)	2.978	2.945(3)	2.932(3)	2.917(3)
–O_C(o)	2.435	2.503(2)	2.547(3)	2.590(3)
–O_D(m)	3.003	3.003(3)	2.998(3)	2.992(4)
	2.634	2.675	2.698	2.722
T_1(o)–O_A	1.745	1.742(2)	1.740(2)	1.742(2)
–O_B	1.738	1.744(2)	1.742(2)	1.740(2)
–O_C	1.735	1.733(2)	1.736(2)	1.735(2)
–O_D	1.742	1.745(2)	1.744(2)	1.741(2)
	1.740	1.741	1.740	1.740
T_1(m)–O_A	1.596	1.595(2)	1.595(2)	1.593(2)
–O_B	1.601	1.598(2)	1.596(2)	1.594(2)
–O_C	1.619	1.619(2)	1.620(2)	1.616(2)
–O_D	1.620	1.616(2)	1.615(2)	1.616(2)
	1.609	1.607	1.607	1.605
T_2(o)–O_A	1.632	1.626(2)	1.624(2)	1.625(2)
–O_B	1.594	1.589(2)	1.588(2)	1.581(2)
–O_C	1.617	1.623(2)	1.622(2)	1.622(2)
–O_D	1.612	1.614(2)	1.616(2)	1.611(2)
	1.614	1.613	1.613	1.610
T_2(m)–O_A	1.643	1.646(2)	1.647(2)	1.647(2)
–O_B	1.616	1.621(2)	1.619(2)	1.616(2)
–O_C	1.599	1.595(2)	1.594(2)	1.594(2)
–O_D	1.601	1.597(2)	1.594(2)	1.595(2)
	1.615	1.615	1.614	1.613

*Data from Wainwright (in Smith,1974)

Although the *a* axis shows the largest variation with temperature, the longest axis of the strain ellipsoid clearly indicates a maximum expansion in a direction 40° away from *a* (Table 7). In addition, the shortest axis, lying approximately in the *b*–*c* plane, indicates a cell contraction in this direction as temperature is raised.

The cell expansion is principally controlled by adjustments of the aluminosilicate framework itself. Na plays a relatively passive role, for reasons to be discussed later. No single parameter adequately explains the orientation of the thermal strain ellipsoid. The response of the structure to changing temperature appears to be controlled by the interaction of at least three factors. First is the greater flexibility of the framework along the *a* crystallographic axis, which is

Table 6. Tiburon low albite: O–*T*–O and *T*–O–*T* bond angles as a function of temperature

		25°C*	500°C	750°C	970°C
$T_1(o)$	ATB	103.0	103.6(1)	103.8(1)	104.0(1)
	ATC	115.9	115.1(1)	114.9(1)	114.8(1)
	ATD	104.3	104.6(1)	104.9(1)	105.0(1)
	BTC	112.0	112.5(1)	112.5(1)	112.6(1)
	BTD	111.2	111.1(1)	111.1(1)	110.9(1)
	CTD	110.1	109.6(1)	109.3(1)	109.2(1)
$T_1(m)$	ATB	109.4	108.9(1)	108.8(1)	108.7(1)
	ATC	112.3	112.7(1)	112.8(1)	113.1(1)
	ATD	107.3	107.5(1)	107.4(1)	107.5(1)
	BTC	108.5	108.2(1)	108.4(1)	108.6(1)
	BTD	111.4	111.5(1)	111.6(1)	111.1(1)
	CTD	108.4	108.0(1)	107.9(1)	107.8(1)
$T_2(o)$	ATB	111.2	111.4(1)	111.5(1)	111.5(1)
	ATC	104.6	104.0(1)	104.0(1)	104.0(1)
	ATD	106.9	107.1(1)	107.0(1)	107.2(1)
	BTC	111.9	112.0(1)	111.7(1)	111.7(1)
	BTD	111.5	111.6(1)	111.9(1)	111.7(1)
	CTD	110.4	110.4(1)	110.4(1)	110.5(1)
$T_2(m)$	ATB	107.2	107.0(1)	106.9(1)	106.7(1)
	ATC	106.0	105.8(1)	105.7(1)	105.5(1)
	ATD	108.5	108.7(1)	108.7(1)	109.0(1)
	BTC	110.3	110.1(1)	110.2(1)	110.5(1)
	BTD	110.3	110.6(1)	110.6(1)	110.6(1)
	CTD	114.3	114.3(1)	114.3(1)	114.2(1)
T1-OA1-T1		141.6	143.0(1)	143.4(1)	143.6(1)
T2-OA2-T2		130.2	131.3(1)	132.0(1)	132.5(1)
T1-OBO-T2		139.7	141.2(1)	142.3(1)	143.9(2)
T1-OBm-T2		160.9	159.9(2)	159.6(2)	159.4(2)
T1-OCO-T2		129.6	130.4(1)	130.6(1)	130.7(1)
T1-OCm-T2		136.0	135.3(1)	135.1(1)	135.2(1)
T1-ODO-T2		134.1	134.7(1)	135.4(1)	136.0(1)
T1-ODm-T2		152.0	151.0(1)	149.9(2)	149.0(2)

*Data from Wainwright (in Smith, 1974)
ATB indicates the O_A-T-O_B angle etc.

the direction of the aluminosilicate "double crankshafts" (Smith, 1974). Two additional factors have a modifying effect on the simple stretching of the crankshafts. There is a tendency for the structure to overcome the collapse about the small Na atom with increasing temperature. Although inhibited by the ordered Si/Al topology, every atom slightly approaches a position of monoclinic geometry (Table 2). This is indicated by a decrease in the obtuse α angle and the approach of β to the ideal sanidine value of 116.0 (or monalbite β = 116.1; Okamura and Ghose, 1975) (Fig. 2.). However, the acute γ angle also decreases, although certainly much less than α and β. This may reflect the modifying effects of Si/Al order. A second restraint on the crankshaft stretching is imposed by the O_{A1} atoms which join adjacent crankshafts in the *c* direction (Fig. 4). Where one crankshaft opens upward, it is joined along the diagonals to an adjacent crankshaft, which opens downward, thus inhibiting one another's freedom of motion. The result appears to be a stretching between the two O_{A1} joins. If so, this action would cause the diagonal $T_2(o)$ atoms to move closer to each other. The direction between these two atoms is also the direction of the negative axis of the thermal expansion ellipsoid.

It should be noted at this point that the sample being analyzed at elevated temperatures remains a nearly completely ordered albite with respect to Si/Al, and is therefore not the equilibrium form at the temperatures of analysis. Increasing Si/Al disorder as temperature is raised will certainly contribute to the structural response of the crystal.

Na anistropy as a function of temperature

As regards the principal problem, that of the Na anistropy, the isotropic equivalent temperature factor is plotted against temperature in degrees Kelvin in Figure 5. Included are the room-temperature data of

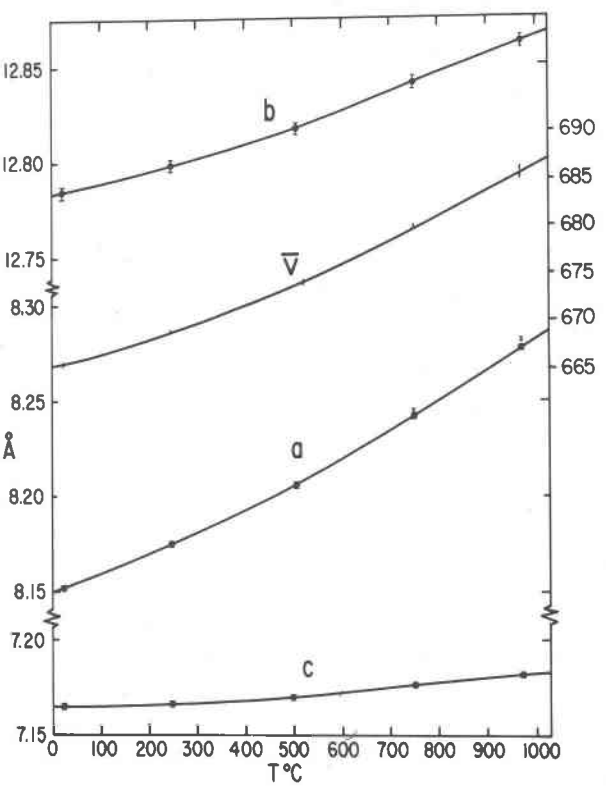

Fig. 1. Cell dimensions and volume of Tiburon albite *vs.* temperature. Error bars represent ± one standard deviation. The curve is fitted to the values measured with increasing temperature. Where the cell dimension measured as temperature was decreased differs from these values by greater than two standard deviations, it is plotted as a separate symbol.

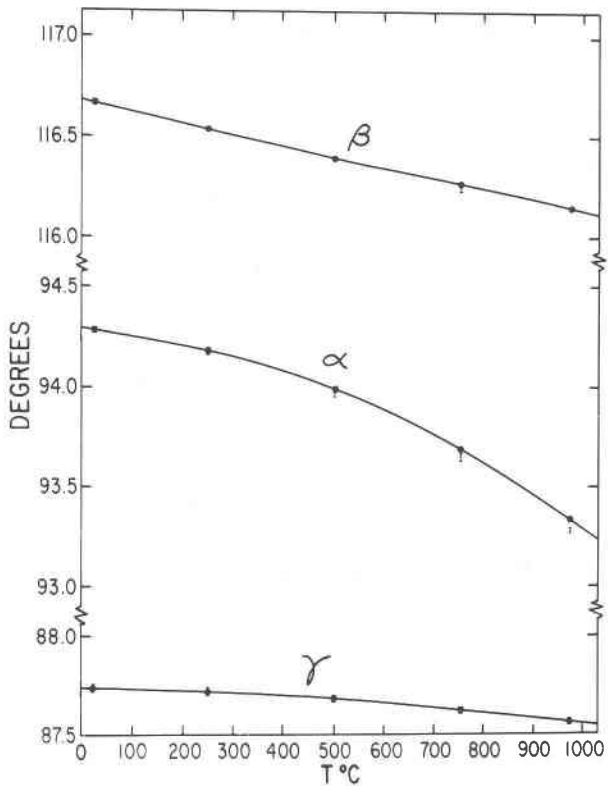

Fig. 2. Cell angles of Tiburon low albite *vs.* temperature. Error bars represent ± one standard deviation.

Wainwright and the 93 K data of Williams and Megaw (1964) as re-refined by Quareni and Taylor (1971). A reasonably good linear fit is demonstrated and extrapolates to $B = 0$ K within error limits. This confirms the hypothesis of Quareni and Taylor (1971) that the Na anisotropy is strictly the result of thermal vibration about a single point. If there were some spatial disorder, B at 0 K would have a magnitude sufficient to encompass the multiple positions. This is

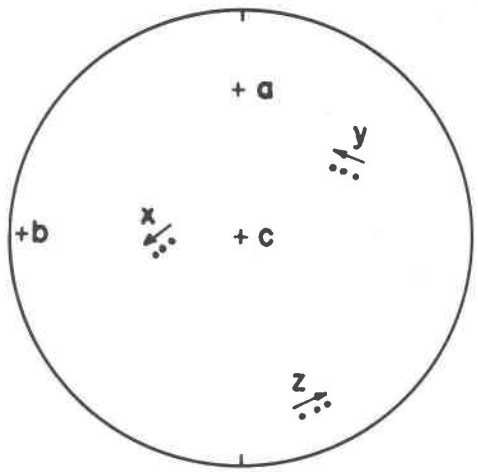

Fig. 3. Stereographic projection of the minimum (x), intermediate (y), and maximum (z) axes of the thermal expansion ellipsoids for Tiburon low albite at 25 → 500°C, 25 → 750°C, and 25 → 970°C respectively in the direction of the arrows. Cell axes are included.

readily demonstrated by the data points for high albite obtained thus far, by Williams and Megaw (1964) at 93 K (hydrothermal synthesis at 700°C), by us at 298, 773, 1023, and 1253 K (Tiburon albite, heat-treated at 1080°C for 60 days), and by Prewitt *et al.* (1976) at 297, 573, 873, 1023, 1173, 1363 and 1378 K on a synthetic high albite (annealed at 1060°C for 40 days). A linear fit to the data extrapolates to a B value of 5.85A² at 0 K. This large B value, at a temperature where thermal motion should be zero, can only be explained by some multiple position effect, a result also obtained by Prewitt *et al.* (1976).

As a check of the results for low albite, R_3, the longest axis of the thermal ellipsoid, was plotted against temperature in degrees Kelvin. If the anisotropy is a result of thermal vibrations, it should also reduce to zero at 0 K. If $(R_3)^2$ is plotted against

Table 7. Tiburon low albite: principal strain components of thermal expansion

Temperature Range, °C	Principal Strain Components per 1°C x10^{-5}	Orientation of Principal Axes: Angle (degrees) with respect to: +a	+b	+c
25–500	2.09(6)	42(2)	71(2)	79(1)
	0.77(6)	125(3)	44(3)	59(2)
	-0.23(6)	110(2)	127(2)	33(2)
25–750	2.32(4)	45(1)	67(1)	78(1)
	0.95(3)	131(1)	50(1)	55(1)
	-0.33(3)	106(1)	131(1)	37(1)
25–970	2.50(3)	48(1)	64(1)	77(1)
	1.07(2)	134(1)	54(1)	53(1)
	-0.47(3)	104(1)	133(1)	40(1)

temperature (Fig. 6), the curve becomes much more linear, like the one for B, and also extrapolates to $(R_3)^2 = 0$ at 0 K. As in the case for B, the units become A^2 *vs.* temperature. The linearity of this relationship is in accordance with the Debye model for thermal motion, which predicts a direct proportionality between temperature and the square of the mean square amplitude of vibration. There is a slight, but consistent, deviation from linearity at higher temperatures, which may be due to changes in the relative strengths of Na–O and T–O bonds or, more likely, restrictions imposed on the Na vibrations by the aluminosilicate cage.

Figure 7 shows the coordination of the Na atom in low albite at 970°C. The thermal displacement ellipsoids of Na and O are included. The R_3 axis for Na is nearly parallel to the b crystallographic axis and normal to the Na–O_{A2} bond, the shortest of the Na–O bonds. This direction permits the maximum movement of the Na atom without obstruction by the neighboring atoms. The high anisotropy of the Na atom in a cage which can accomodate the much larger K atom seems quite reasonable in this light. A subservient role of Na with respect to cell expansion is indicated.

Isotropic temperature factors, Na–O and T–O bond lengths and angles as a function of temperature

Equivalent isotropic temperature factors for Si, Al, and O are also plotted against temperature (Fig. 8) and likewise show linear fits extrapolating to $B = 0$ at 0 K. The average oxygen B value actually extrapolates to $B = 0.1$ A² at 0 K, but this is within the error limits of a zero value. If this magnitude is real, it may result from unequal Si–O and Al–O bond lengths combined with incomplete Si/Al order.

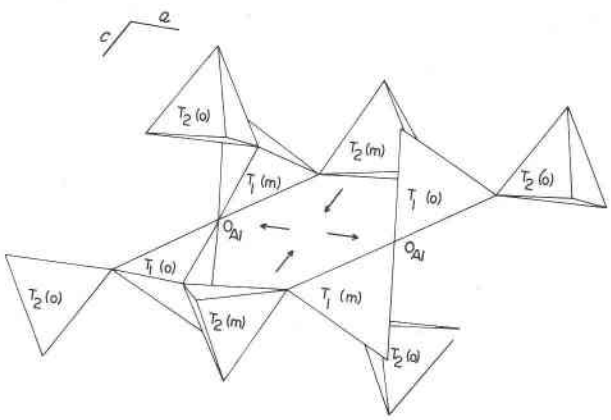

Fig. 4. Adjacent tetrahedral crankshaft chains joined by O_{A1} links. Arrows indicate stretching direction between the O_{A1} links and the resulting approach of the diagonal $T_2(m)$ atoms.

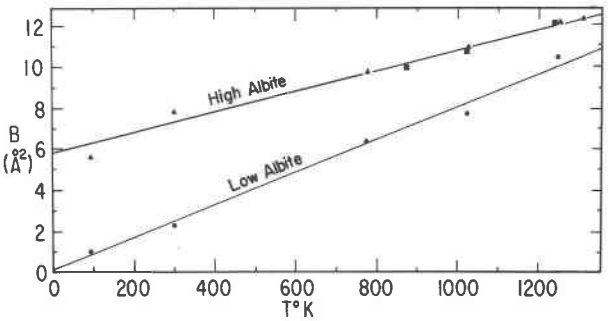

Fig. 5. Isotropic equivalent temperature factor (B) for the Na atom in high and low albite *vs.* temperature. Dots represent low albite, triangles represent our data on high albite, and squares represent the data of Prewitt *et al.* (1976) on high albite.

The bond angles as a function of temperature display a quite linear fit, indicating a smooth, continuous change over the observed temperature range. Rarely does an O–T–O angle change by more than half a degree over the observed temperature range, while changes of three or more degrees are quite common for T–O–T angles. Thus it is clear that the angles between adjacent tetrahedra are more flexible and respond more readily to lattice strain than do angles within a tetrahedron.

Most of the Na–O bond lengths, plotted as a function of temperature (Fig. 9), show a substantial increase as temperature is raised. The two longest bonds, however, become shorter with increasing temperature. This apparently results from a straightening of the aluminosilicate cage, which may be thought of as collapsed about the small Na atom, especially at low temperatures. Note that there is no consistent correlation between the size of a Na–O bond length and the magnitude of the change in that bond length with temperature. If one expected the Na atom to participate in the thermal response of the structure in a dominant fashion, the shorter Na–O bond lengths ought to increase more readily than the longer ones, which is not the case.

In contrast to the expansion of Na–O bonds, the T–O bonds remain nearly constant or decrease slightly with increasing temperature. This behavior is

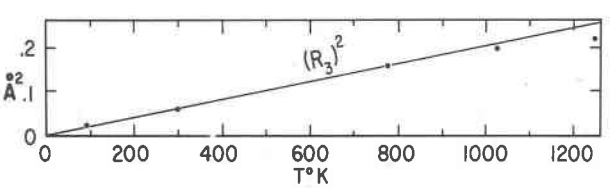

Fig. 6. Tiburon low albite. Long axis of the Na thermal ellipsoid (R_3) squared *vs.* temperature.

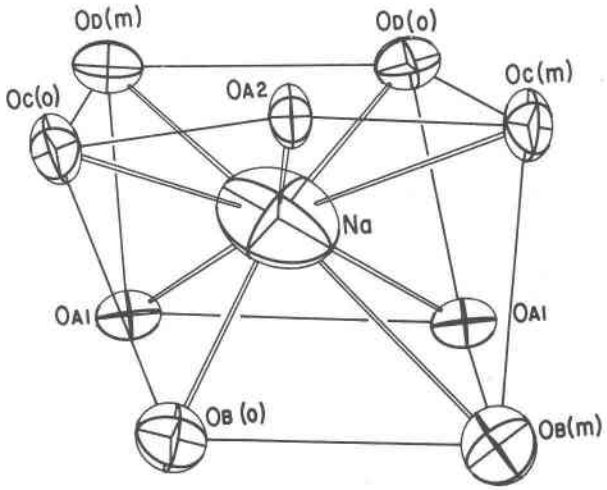

Fig. 7. Na atom coordination and thermal ellipsoid in Tiburon low albite at 970°C.

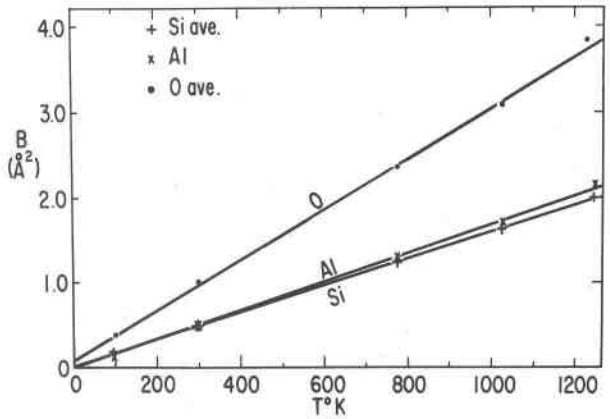

Fig. 8. Isotropic equivalent temperature factors for Al,Si (average), and O(average) for low Tiburon albite *vs.* temperature.

unexpected, since the predominant cell response of this framework silicate is expansion. Similar apparent contractions of Si–O bonds with increasing temperature have been observed in other silicate minerals (Smyth and Burnham, 1972; Smyth, 1973, 1974; Ohashi, 1973; Sueno *et al.*, 1973 a, b; Ohashi and Finger, 1975; Finger and Ohashi, 1976; Hazen, 1976), which have been attributed to: (1) the strength of the Si–O bond, (2) complex *M*–O–Si interactions, and (3) thermal vibration effects.

Although the Si–O and Al–O bonds are indeed stronger than Na–O bonds, for these bonds to remain constant requires a symmetrical potential energy well. For them to actually decrease, the outer wall must be steeper than the inner one. Although there are no direct theoretical constraints, the possibility of the electronic interaction matching or surpassing that of the coulomb nuclear repulsions as a function of the

Table 8. Tiburon low albite: corrected Na–O and *T*–O bond lengths as a function of temperature

		500°C					750°C					970°C				
		Uncor-rected	Lower	Riding	Non-correl.	Upper	Uncor-rected	Lower	Riding	Non-correl.	Upper	Uncor-rected	Lower	Riding	Non-correl.	Upper
Na	$-O_{A1}$	2.739	2.744	2.757	2.776	2.807	2.765	2.771	2.789	2.812	2.854	2.788	2.796	2.817	2.847	2.899
	$-O'_{A1}$	2.609	2.617	2.634	2.653	2.689	2.649	2.659	2.680	2.705	2.751	2.684	2.695	2.721	2.751	2.806
	$-O_{A2}$	2.412	2.424	2.445	2.464	2.504	2.439	2.454	2.481	2.506	2.559	2.467	2.483	2.515	2.546	2.609
	$-O_B$(o)	2.511	2.519	2.538	2.562	2.606	2.556	2.565	2.589	2.620	2.676	2.616	2.626	2.653	2.690	2.755
	$-O_C$(o)	2.945	2.948	2.960	2.979	3.010	2.932	2.937	2.952	2.977	3.018	2.917	2.922	2.942	2.974	3.026
	$-O_D$(o)	2.503	2.510	2.530	2.553	2.596	2.547	2.557	2.581	2.611	2.665	2.590	2.600	2.628	2.664	2.727
	$-O_D$(m)	3.003	3.004	3.010	3.031	3.057	2.998	3.000	3.009	3.035	3.071	2.992	2.994	3.007	3.040	3.085
T_1(o)	$-O_A$	1.742	1.744	1.752	1.772	1.800	1.740	1.743	1.754	1.780	1.817	1.742	1.745	1.759	1.792	1.838
	$-O_B$	1.744	1.747	1.756	1.775	1.804	1.742	1.745	1.758	1.783	1.821	1.740	1.744	1.761	1.792	1.840
	$-O_C$	1.733	1.734	1.742	1.761	1.788	1.736	1.738	1.748	1.773	1.809	1.735	1.738	1.751	1.782	1.826
	$-O_D$	1.745	1.747	1.756	1.774	1.801	1.744	1.747	1.759	1.783	1.818	1.741	1.744	1.759	1.788	1.831
T_1(m)	$-O_A$	1.595	1.597	1.607	1.627	1.657	1.595	1.598	1.611	1.638	1.677	1.593	1.597	1.614	1.647	1.696
	$-O_B$	1.598	1.603	1.618	1.637	1.670	1.596	1.604	1.623	1.648	1.692	1.594	1.603	1.626	1.657	1.711
	$-O_C$	1.619	1.621	1.630	1.649	1.677	1.620	1.622	1.634	1.659	1.696	1.616	1.620	1.635	1.666	1.712
	$-O_D$	1.616	1.620	1.633	1.650	1.681	1.615	1.620	1.636	1.660	1.699	1.616	1.622	1.642	1.671	1.719
T_2(o)	$-O_A$	1.626	1.627	1.631	1.653	1.679	1.624	1.625	1.631	1.659	1.694	1.625	1.626	1.634	1.669	1.712
	$-O_B$	1.589	1.592	1.603	1.620	1.649	1.588	1.592	1.606	1.630	1.667	1.581	1.586	1.605	1.634	1.682
	$-O_C$	1.623	1.624	1.633	1.653	1.681	1.622	1.624	1.636	1.661	1.699	1.622	1.626	1.640	1.672	1.719
	$-O_D$	1.614	1.618	1.630	1.649	1.681	1.616	1.621	1.637	1.662	1.703	1.611	1.617	1.637	1.667	1.718
T_2(m)	$-O_A$	1.646	1.647	1.651	1.672	1.698	1.647	1.648	1.654	1.682	1.716	1.647	1.648	1.657	1.691	1.734
	$-O_B$	1.621	1.627	1.641	1.659	1.692	1.619	1.627	1.645	1.669	1.712	1.616	1.624	1.647	1.677	1.729
	$-O_C$	1.595	1.597	1.605	1.625	1.654	1.594	1.597	1.609	1.635	1.673	1.594	1.597	1.612	1.644	1.691
	$-O_D$	1.597	1.600	1.611	1.629	1.658	1.594	1.598	1.612	1.636	1.674	1.595	1.599	1.615	1.646	1.692

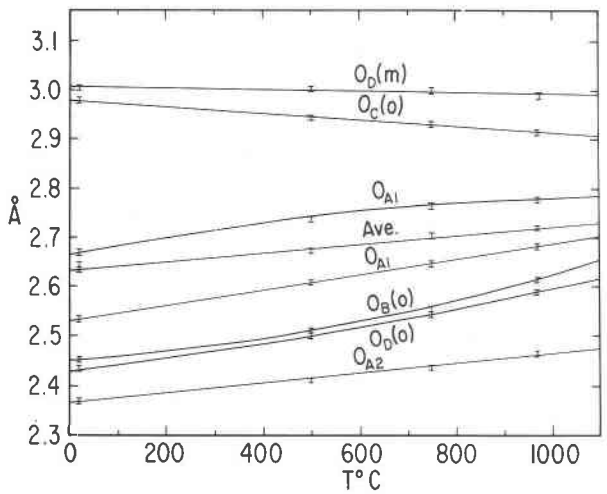

Fig. 9. Na–O bond lengths in Tiburon low albite *vs.* temperature. Error bars represent ± one standard deviation.

atomic separations is prohibitively remote. This behavior has never been observed in nature for any diatomic molecule, including Si–O and Al–O (see Herzberg, 1950).

The possibility may yet exist that a shared bond may transfer energy to a *T*–O bond at elevated temperatures and thereby decrease the bond length. Thus

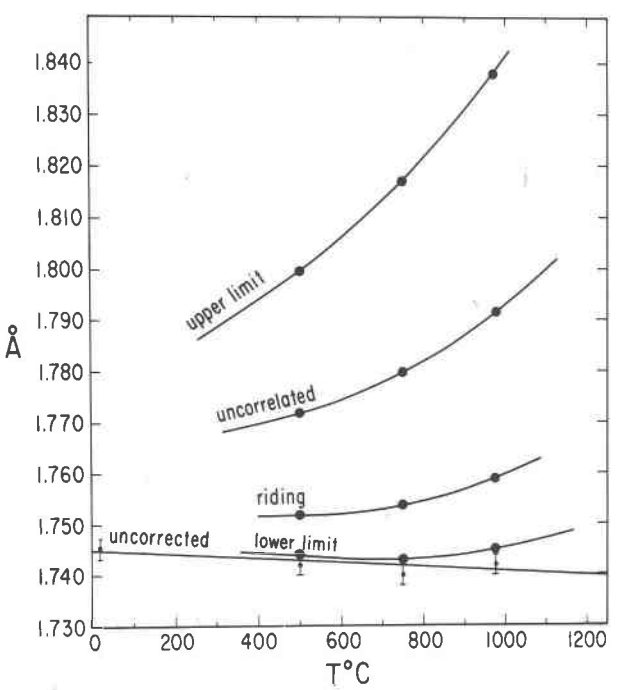

Fig. 10. An example of the temperature corrections of Busing and Levy (1964) applied to a typical *T*–O bond length in Tiburon low albite as a function of temperature. The uncorrected values with ± one standard deviation are included for reference.

Appendix. Table 1. Linear and second-order coefficients for temperature dependent data*

	A x10^{-4}	correl. coeff.	A' x10^{-5}	B' x10^{-8}
Cell				
a	1.37	.995	6.59	4.47
b	.84	.997	4.74	2.26
c	.18	.961	-1.07	1.88
α	-10.75	.973	28.54	-85.25
β	-5.54	.999	-64.30	5.63
γ	-1.92	.970	4.30	-15.28
V	213.81	.996	1086.76	658.63
Temperature Factors				
Na B	79.76	1.0		
R_3	2.42	.982		
$(R_3)^2$	1.74	.993		
Al B	17.00	1.0		
Si B	15.63	1.0		
$O_{ave.}$ B	29.52	1.0		
Angles				
T_1(o)-ATB	10.40	.993		
ATC	-11.93	.970		
ATD	7.71	.990		
BTC	6.25	.937		
BTD	-2.74	.884		
CTD	-9.88	.992		
T_1(m)-ATB	-7.46	.974		
ATC	8.03	.987		
ATD	1.79	.758		
BTC	0.82	.194		
BTD	-1.84	.346		
CTD	-6.38	.984		
T_2(o)-ATB	3.38	.970		
ATC	-6.51	.881		
ATD	2.62	.822		
BTC	-2.54	.688		
BTD	3.06	.727		
CTD	0.83	.672		
T_2(m)-ATB	-5.04	.982		
ATC	-5.04	.982		
ATD	4.65	.916		
BTC	1.52	.361		
BTD	3.26	.881		
CTD	-0.83	.672		
T-OA1-T	21.73	.979		
T-OA2-T	24.54	.999		
T-OBo-T	42.82	.980		
T-OBm-T	-16.14	.984		
T-OCo-T	11.93	.970		
T-OCm-T	-9.19	.913		
T-ODo-T	19.94	.979		
T-ODm-T	-31.61	.983		

*Curves fitted by Bio-medical polynomial regression computer program (BMD05R). Curves have the form: $Y=X+AT$ and $Y=X+A'T+B'T^2$

the greatly lengthened Na–O bonds might shift energy to the *T*–O bonds via the common oxygen. Such interactions have been proposed for Mg–O–Si interactions in olivine (Hazen, 1976). As most interactions are *T*–O–*T*, and *M*–O bonds are fewer in feldspars than in olivine, the nature of the *M*–O–Si interaction should be clearer. If this interaction is responsible for the observed *T*–O behavior, the magnitude of the change in *T*–O bond length should show a strong correlation with the magnitude of the change in the neighboring Na–O bond length. Table 5 and the regression equations in the appendix indicate no such correlation. Nor, for that matter, is there a correlation between the magnitude of the *T*–O bond length change and the size of the neighboring Na–O bond

Appendix. Table 2. Linear coefficients ($A \times 10^{-6}$) for bond length *vs.* temperature data including thermal corrections of Busing and Levy (1964)*

	uncorrected	lower	riding	uncor-related	upper	correl. coeff. for upper
Na-O_{A1}	12.65	11.06	12.77	15.09	19.56	1.0
O^{A1}	15.77	16.60	18.51	20.85	24.89	1.0
O^{A2}	10.25	12.54	14.88	17.43	22.33	1.0
O_B(o)	16.59	22.67	24.38	27.14	31.62	.997
O_C(o)	-6.40	-5.51	-3.82	-1.06	3.40	.999
O_D(o)	16.26	19.14	20.84	23.61	27.87	1.0
O_D(m)	-1.10	-2.12	-0.63	1.91	5.95	.999
T_1(o)-O_A	-0.40	0.20	1.47	4.23	8.06	.995
O_B	0.24	-0.64	1.06	3.61	7.64	.998
O_C	0.06	0.87	1.93	4.48	8.09	1.0
O_D	-0.04	-0.62	0.65	2.99	6.39	.999
T_1(m)-O_A	-0.27	0.01	1.49	4.26	8.06	1.0
O_B	-0.73	0.01	1.71	4.26	8.73	1.0
O_C	-0.21	-0.20	1.08	3.63	7.45	1.0
O_D	-0.47	0.42	1.90	4.46	8.07	.998
T_2(o)-O_A	-0.81	-0.23	0.62	3.38	7.00	.996
O_B	-1.24	-1.25	0.44	3.00	7.03	1.0
O_C	0.53	0.42	1.48	4.02	8.07	.998
O_D	0.05	-0.18	1.52	3.86	7.89	.997
T_2(m)-O_A	0.45	0.22	1.27	4.04	7.65	.999
O_B	0.05	-0.62	1.28	3.83	7.87	1.0
O_C	-0.56	0.00	1.49	4.04	7.87	1.0
O_D	-0.71	-0.23	0.84	3.60	7.22	.997

*There is no room temperature data available with temperature corrections. Therefore the curves for the corrected bondlengths are fitted to only 3 data points while the room T curves are for 4.

length itself. Data on the structure of quartz (Young, 1962) also show an apparently constant or slightly decreasing Si–O bond length as temperature is raised, with no octahedral atoms in the structure to donate bond strength.

We believe that the apparent contraction of many *T*–O bonds in silicates probably results from errors in measurement caused by thermal motion. The refinement method used for X-ray data produces as atomic positions the centers of ellipsoids fitted to the average electron-density distribution for that atom. As pointed out by Busing and Levy (1964), the calculated distance between two such static positions may differ from the time-averaged mean separation of the true vibrating atom centers.

The bond lengths, corrected using the four modeled interactions (after Busing and Levy, 1964), are listed in Table 8. To illustrate the magnitude of these corrections to the present study, Figure 10 shows how the various corrections affect the computed length of a single *T*–O bond, in this case T_1(o)–O_{A1}, over the temperature range studied. Note that the *T*–O distance increases with increasing temperature for most corrected curves. This is indeed true for all *T*–O bonds.

Until data on the distribution of individual atom pairs during vibration becomes available, we cannot accurately determine the actual bond length within the range of the upper and lower limits. Thus these limits effectively become the error limits of the bond-length estimation. At high temperature this error can be more than 50 times the standard deviation error due to measurement. At 970°C this range is generally about 6 percent of the uncorrected bond length. In addition, bond-angle calculations involve uncertainties in the joint distribution of three atoms. It is thus virtually impossible to correct bond angles with any accuracy when large thermal motions are involved. Hopefully infrared and Raman spectroscopic techniques at elevated temperatures will supply much-needed data concerning the nature of these vibrations.

Summary and conclusions

1. The thermal strain ellipsoids of low albite indicate cell expansions in directions significantly different from the axial directions. The minimum expansion direction actually amounts to a contraction of the cell in certain directions as temperature is raised. No single structural parameter adequately explains the cell-expansion behavior. Presumably three factors contribute to the observed responses: (1) the greater flexibility of the framework along the "double crankshaft" chains, (2) restrictions imposed on the afore-

mentioned flexibility by the linking of adjacent crankshafts along the *c* direction, and (3) a small, but progressive approach toward monoclinic geometry.

2. The marked anisotropy associated with the Na position in low albite results solely from highly anisotropic thermal vibration about a single node as suggested by Quareni and Taylor (1971). Results on high albite indicate some form of positional disorder as well.

3. When dealing with bond lengths and angles in crystalline solids at elevated temperatures, corrections for the effects of thermal motion must be considered. As it is presently impossible to describe completely the true mutual distribution of all the atom centers as they vibrate, rather large uncertainties may result. In this study these corrections are sufficient to reverse the apparent trend toward decreasing *T*–O bond lengths with increasing temperature in most of the uncorrected observations.

Acknowledgments

We thank those people who contributed time, equipment, or technical advice to this study: Dr. B. W. Evans, for his sample of Tiburon albite; Mr. James Carter; Mr. M. Burton, Mr. Val Kiefer, Dr. James Blacic, and Dr. Stewart McCallum, for technical assistance. Dr. L. W. Finger, Geophysical Laboratory, Washington, D. C. kindly calculated the thermal strain ellipsoids. Drs. R. M. Hazen and L. W. Finger critically read the manuscript and offered suggestions for improvement.

References

Bond, W. L. (1951) Making small spheres. *Rev. Sci. Instrum., 22,* 344–345.

Busing, W. R. and H. A. Levy (1964) The effect of thermal motion on the estimation of bond lengths from diffraction measurements. *Acta Crystallogr., 17,* 142–146.

Cromer, D. T. and J. B. Mann (1968) X-ray scattering factors computed from numerical Hartree-Fock wave function. *Acta Crystallogr., A24,* 321–324.

——— and D. Liberman (1970) Calculation of anomalous scattering factors for X-rays. *J. Chem. Phys., 53,* 1891–1898.

Ferguson, R. B., P. J. Trail and W. H. Taylor (1958) The crystal structures of low-temperature and high-temperature albites. *Acta Crystallogr., 11,* 331–348.

——— and Y. Ohashi (1976) Thermal expansion of diopside. *Am. Mineral., 61,* 303–310.

Finger, L. W. (1969) Determination of cation distribution by least-squares refinement of single-crystal X-ray data. *Carnegie Inst. Wash. Year Book, 67,* 216–217.

Hazen, R. M. (1976) Effects of temperature and pressure on the crystal structure of forsterite. *Am. Mineral., 61,* 1280–1293.

Herzberg, G. (1950) *Molecular Spectra and Molecular Structure, I. Spectra of Diatomic Molecules.* Van Nostrand, New York.

Ohashi, Y. (1973) *High Temperature Structural Crystallography of Synthetic Pyroxenes (Ca,Fe)SiO$_3$.* Ph.D. Thesis, Harvard University.

——— and L. W. Finger (1973) Lattice deformations in feldspars. *Carnegie Inst. Wash. Year Book, 72,* 569–573.

——— and ——— (1975) Refinement of the crystal structure of sanidine at 25° and 400°C. *Carnegie Inst. Wash. Year Book, 73,* 539–544.

Okamura, F. P. and S. Ghose (1975) Analbite→monalbite transition in a heat-treated twinned Amelia albite. *Contrib. Mineral. Petrol., 50,* 211–216.

Prewitt, C. T., S. Sueno and J. J. Papike (1974) Models for albite in different structural states. *EOS Trans. Am. Geophys. Union, 55,* 464.

——— (1976) The crystal structures of high albite and monalbite at high temperatures. *Am. Mineral., 61,* 1213–1225.

Quareni, S. and W. H. Taylor (1971) Anisotropy of the sodium atom in low albite. *Acta Crystallogr., 27B,* 281–285.

Ribbe, P. H., H. D. Megaw, W. H. Taylor, R. B. Ferguson and R. J. Traill (1969) The albite structures. *Acta Crystallogr., 25B,* 1503–1518.

Smith, J. V. (1974) *Feldspar Minerals,* Vol. 1. Springer-Verlag, New York.

Smyth, J. R. (1973) An orthopyroxene structure up to 850°C. *Am. Mineral., 58,* 636–648.

——— (1974) The high-temperature crystal chemistry of clinohypersthene. *Am. Mineral., 59,* 1069–1082.

——— and C. W. Burnham (1972) The crystal structures of high and low clinohypersthene. *Earth Planet. Sci. Lett., 14,* 183–189.

Sueno, S., M. Cameron and C. T. Prewitt (1973a) The orthoferrosilite structure (abstr.). *Geol. Soc. Am. Abstr. Programs, 5,* 829–830.

———, C. T. Prewitt and J. J. Papike (1973b) High temperature crystal chemistry of albite (abstr.). *Trans. Am. Geophys. Union 54,* 1230.

Willaime, C., W. L. Brown and M. C. Pernaud (1974) On the orientation of the thermal and compositional strain ellipsoids in feldspars. *Am. Mineral., 59,* 457–464.

Williams, P. P. and H. D. Megaw (1964) The crystal structures of high and low albites at −180°C. *Acta Crystallogr., 17,* 882–890.

Winter, J. K. and S. Ghose (1977) A reinvestigation of the analbite–monalbite transition at high temperatures. *EOS Trans. Am. Geophys. Union, 58,* in press.

Young, R. A. (1962) *Mechanism of the Phase Transition in Quartz.* Final Report, Solid State Sciences Division, Air Force Office of Scientific Research (Project A-447).

Manuscript received, January 3, 1977; accepted for publication, May 18, 1977.